IOPscience iopscience.iop.org

Home Search Collections Journals About Contact us My IOPscience

Disordering and dopant behaviour in Au^{+}-ion-irradiated AlN

This article has been downloaded from IOPscience. Please scroll down to see the full text article.

2007 J. Phys.: Condens. Matter 19 356207

(http://iopscience.iop.org/0953-8984/19/35/356207)

View the table of contents for this issue, or go to the journal homepage for more

Download details:
IP Address: 129.252.86.83
The article was downloaded on 29/05/2010 at 04:33

Please note that terms and conditions apply.

J. Phys.: Condens. Matter **19** (2007) 356207 (10pp) doi:10.1088/0953-8984/19/35/356207

Disordering and dopant behaviour in Au^+-ion-irradiated AlN

W Jiang[1], **I-T Bae and W J Weber**

Pacific Northwest National Laboratory, Richland, WA 99352, USA

E-mail: weilin.jiang@pnl.gov

Received 28 April 2007, in final form 1 July 2007
Published 2 August 2007
Online at stacks.iop.org/JPhysCM/19/356207

Abstract
Single-crystal AlN films on SiC were irradiated at 145 K with 1.0 MeV Au^+ ions in a wide range of ion fluences. The accumulation of disorder on both the Al and N sublattices in AlN has been investigated *in situ* using conventional Rutherford backscattering spectrometry (RBS) and non-RBS along the ⟨0001⟩-axial channelling direction. The results suggest that a disorder saturation stage is attained following an initial disorder increase at doses less than 10 displacements per atom (dpa). A continuously amorphized layer was not formed in AlN for doses up to 208 dpa. Similar disordering behaviour is observed for the Al and N sublattices. The lattice disorder produced at 145 K is thermally stable at room temperature; further irradiation does not induce disorder recovery. The microstructures in the irradiated AlN exhibit both amorphous and crystalline domains at the stage of disorder saturation. The implanted Au does not show significant redistribution during the ion irradiation or room-temperature annealing.

(Some figures in this article are in colour only in the electronic version)

1. Introduction

Aluminium nitride (AlN) has a direct bandgap of 6.2 eV at room temperature, which is the largest among the well-studied wide-bandgap semiconductors. The material and its alloys have been the subject of extensive research for advanced optoelectronic and photonic applications [1]. Recently, an AlN light-emitting diode (LED) with an unprecedented wavelength as small as 210 nm (deep ultraviolet) was successfully fabricated based on both Mg (p-type) and Si (n-type) doping [2]. In addition, AlN also has been proposed as an electrical insulator for fusion reactors because of its high resistivity, small neutron capture cross sections, high melting point, and good thermal, mechanical and chemical stabilities [3, 4].

[1] Author to whom any correspondence should be addressed.

 © 2007 IOP Publishing Ltd Printed in the UK

Donor and acceptor dopants must be incorporated into the AlN structure prior to device applications. Traditional doping by diffusion is not an option for AlN due to its high thermal stability. Ion implantation has proven to be an effective method for dopant incorporation in many semiconductor materials. It offers the advantage to implant nearly any combination of dopants and solid materials with precise control of the dopant concentration, area and depth. However, ion implantation produces lattice disorder that is detrimental to device performance. A successful application of ion implantation depends on a fundamental understanding of the accumulation and recovery of ion-beam-induced disorder, as well as the dopant behaviour in the material. Ion implantation also provides a convenient means to study radiation effects in AlN and to assess or predict its performance under high-radiation environments, which are important for fusion energy systems. Over the past decade, significant research efforts have been devoted to the study of implantation effects in similar wide-bandgap materials, such as gallium nitride (GaN) and silicon carbide (SiC). In contrast, few reports [5–8] on ion-implantation-induced damage and dopant behaviour in AlN are available. The current knowledge about the disordering and amorphization processes in AlN is still very limited. This study reports for the disorder accumulation and dopant behaviour in AlN using both ion backscattering in channelling geometry and transmission electron microscopy (TEM).

2. Experimental procedures

The undoped AlN single-crystal films ($\sim$14.0 μm thick) used in this study were epitaxially grown on $\langle 0001 \rangle$-oriented 6H-SiC substrates. Both ion irradiation and disorder measurements were performed using the 3.0 MV tandem accelerator within the Environmental Molecular Sciences Laboratory (EMSL) at the Pacific Northwest National Laboratory (PNNL) [9, 10]. Specimens were implanted 60° relative to the surface normal using 1.0 MeV Au^+ ions to various fluences ranging from 2.3 to 424 Au^+ nm^{-2} at 145 K. The irradiation geometry was chosen to produce shallow damage and implants that could be readily measured *in situ* by He^+-ion backscattering, while the low temperature provided a condition to minimize simultaneous defect recovery during the irradiation. The typical ion flux for the irradiation was of the order of 0.12 Au^+ nm^{-2} s^{-1}.

Following irradiation, channelling analyses were performed *in situ* using 2.0 MeV He^+ Rutherford backscattering spectrometry along the $\langle 0001 \rangle$ axial channelling direction (RBS/C) at a scattering angle of 150°. The irradiated sample was maintained at the irradiation temperature (145 K) until the RBS/C analysis at the low temperature was completed. Thermal annealing in vacuum was followed at room temperature for 72 h. The same RBS/C method was used to study the temperature response of the disorder in AlN. Simultaneous analysis of the disorder on both the Al and N sublattices in AlN was then conducted using the enhanced backscattering of $^{14}N(\alpha, \alpha)^{14}N$ at an incident energy of $E_\alpha = 3.5$ MeV and a scattering angle of 150°. The depth resolution of Al at the surface for the non-RBS/C analysis corresponds to $\sim$35 nm, which is slightly worse than that ($\sim$27 nm) for the conventional 2.0 MeV He^+ RBS/C method. The analysing beam had an angular dispersion of less than 0.05° and induced negligible damage in the investigated depth region during the channelling analyses. The random-equivalent spectrum was obtained by averaging four spectra collected in the virgin (unirradiated) and the highest-fluence (424 Au^+ nm^{-2}) areas with fixed polar angles of $-7°$ and $+7°$ off the surface normal, respectively, while the tilting angle was rotating back and forth in a range from $-3°$ to $+3°$. Note that the arithmetic mean of the two AlN spectra from the implanted area is nearly identical with that from the virgin area except for the slightly lower scattering yields in the surface region (30–130 nm), where a high Au concentration is present.

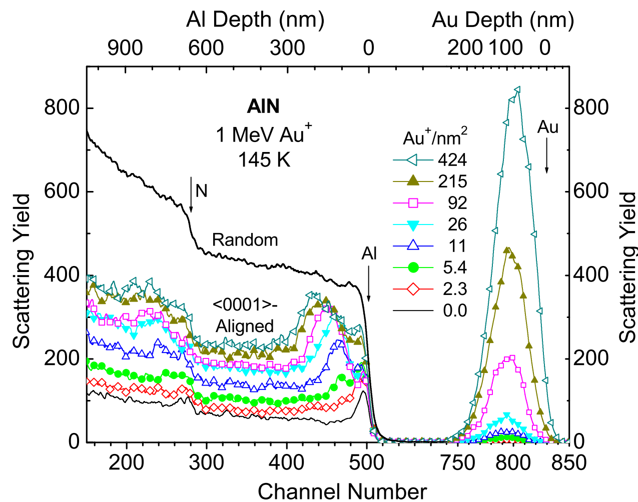

Figure 1. A sequence of the selected 2.0 MeV He^+ RBS/C spectra for a ⟨0001⟩-oriented AlN film (∼14 μm thick) on 6H-SiC irradiated 60° off the surface normal with 1.0 MeV Au^+ ions at 145 K. Also included are an average random spectrum and a ⟨0001⟩-aligned spectrum from a virgin area.

A cross-sectional thin foil of AlN irradiated to 366 Au^+ nm^{-2} at 145 K and stored at room temperature was prepared for TEM examination by standard tripod wedge polishing, followed by 4.0 and 2.5 keV Ar^+ ion-beam thinning to electron transparency. One piece of virgin AlN was glued face-to-face with the irradiated sample. The Ar^+-ion sputtering process was carried out at room temperature without causing observable lattice disorder to the TEM samples. The TEM experiment was conducted using a JEOL 2010 microscope at EMSL under an operating voltage of 200 kV. The specified point-to-point resolution was 0.194 nm. All images (1024 pixels × 1024 pixels) were digitally recorded with a slow-scan charge-coupled device camera.

3. Results and discussion

3.1. Disorder accumulation and stability

A series of 2.0 MeV He^+ RBS/C spectra for AlN irradiated to various Au^+ fluences at 145 K is shown in figure 1. Some of the spectra for the intermediate fluences are omitted in the figure for clarity. Also included in figure 1 are both an average random spectrum (see section 2) and a ⟨0001⟩-aligned spectrum from a virgin area. The depth scales on the upper abscissa for elements Al and Au are referenced to the atomic density of the AlN single crystal (3.26 g cm^{-3}). The minimum yield χ_{min} obtained from the ratio of the aligned virgin spectrum to the random one just behind the surface peak is ∼10%. This is a relatively large value compared to what is typically a few per cent for nearly defect-free AlN single crystals. The main reason for this is the presence of an amorphous surface layer (∼20 nm thick), which has been observed from the TEM experiment in this study (data not shown). However, the as-received AlN in the deeper region has a high crystalline quality, as confirmed by the TEM results (see section 3.2). The random spectrum in figure 1 corresponds to a yield level from an amorphous AlN. From figure 1, the backscattering yields from the implanted Au are well resolved from the AlN spectra, which allows for a simultaneous analysis of lattice disorder and dopant profiles. In addition, the peak areas of the Au have been used for an accurate

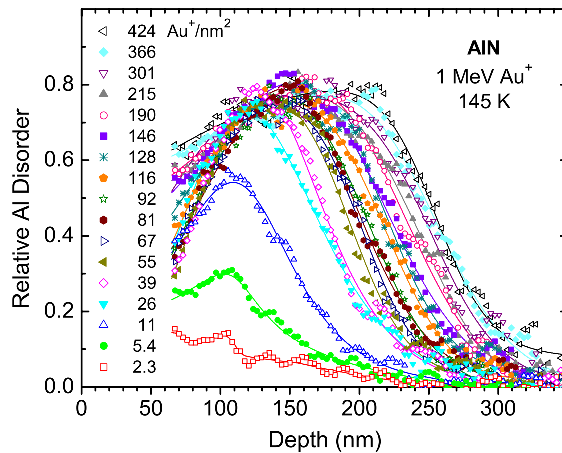

Figure 2. Depth profiles of the relative disorder on the Al sublattice in AlN obtained from the spectra shown in figure 1 and other unplotted spectra. The solid lines are the spline fits to the data.

determination of the relative ion fluence. It should be noted that there was a negligible depth shift of the Au peak when RBS was performed along the random orientation (∼7° off the surface normal). This may be due to the fact that the total energy loss of the He^+ ions occurs primarily in the outgoing path; a small reduction in the stopping powers of the incident channelled He^+ ions does not noticeably modify the depth scaling.

Based on the RBS/C spectra shown in figure 1, the relative disorder on the Al sublattice is obtained through an iterative procedure [11–13], where the dechannelling yield is assumed to be proportional to the level of structural disorder. The experimental results of the relative Al disorder for ion fluences ranging from 2.3 to 424 Au^+ nm^{-2} are shown in figure 2 as a function of depth. Fully amorphized and defect-free phases correspond to unity and zero, respectively, on the vertical scale. At 5.4 Au^+ nm^{-2}, the damage peak is well defined with the peak maximum located at ∼104 nm. The damage peak position gradually shifts to a larger depth as the ion fluence increases in the low-fluence regime. This behaviour may suggest that Al interstitials diffused towards the bulk during the Au^+ irradiation at 145 K. Above a fluence of 26 Au^+ nm^{-2}, the disorder tends to saturate at a level of ∼0.75. The observed profile broadening in figure 2 is largely a result of the disorder saturation over the depth, which is consistent with the disorder saturation over the local dose, as will be discussed below. Full amorphization that can be detected by ion channelling does not occur up to the highest fluence (424 Au^+ nm^{-2}) applied in this study.

In order to estimate the local dose in displacements per atom (dpa), the displacement rate as a function of depth is needed. In this study, the displacement rate has been obtained from the SRIM2006 simulation [14] under the assumption of threshold displacement energy of 50 eV for both Al and N sublattices in AlN [15]. The dose has a linear dependence on ion fluence with a conversion factor of 0.4912 dpa/(ion nm^{-2}) at the damage peak (104 nm). It should be pointed out that the simulation used the database of stopping powers for Au^+, Al^+ and N^+ ions in AlN in a low-energy range (a few eV–1 MeV). In general, the stopping power values for particles at low velocities are not as accurate because there are very few experimental data available for fitting the parameters in the SRIM2006 package. Thus, it is not anticipated that the depth scales for both the ion projected range and the displacement rate are precise from the simulation. A depth correction followed by a normalization procedure should be used in order

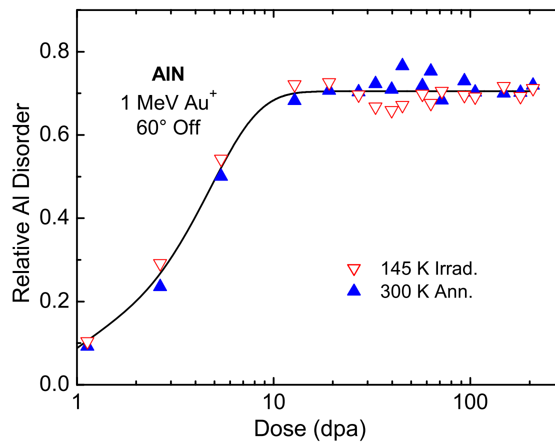

Figure 3. Relative disorder on the Al sublattice, observed along the ⟨0001⟩ axis, as a function of dose at the depth of 104 nm in AlN irradiated at 145 K (downward triangles) and annealed in vacuum at room temperature for 72 h (upward triangles), respectively.

to obtain a more accurate dose at any given depth. In addition, sputtering effects also modify the depth scale, particularly for MeV heavy ions. More discussion regarding the corrections for depth, dose and dopant profiles will be provided in a separate paper.

The dose dependence of the relative Al disorder at the depth of 104 nm in AlN irradiated at 145 K is shown in figure 3. There is a gradual increase in the disorder below a dose of 10 dpa, followed by disorder saturation at the level of ~0.7 at higher doses up to 208 dpa. From the ion-channelling analysis, full amorphization is not observed under the irradiation conditions. The results for the same sample stored at room temperature for 72 h are also included in figure 3. The two sets of data fall on the same curve within experimental error. Thus, there is not a measurable defect recovery at room temperature for AlN under experimental conditions. The stability of the defects in AlN at room temperature is expected because a previous report [6] has indicated that Au^+-ion-implantation-induced defects in AlN are stable up to 1273 K.

The gradual increase in the disorder level at low doses is attributed primarily to elastic collisions induced by the energetic Au^+ ions, which cause atomic displacements from the lattice sites. Apparently, the results in figure 3 indicate that Frankel-pair recombination in AlN at 145 K is less efficient than the defect production during the Au^+-ion irradiation below a dose of 10 dpa. In addition to the generation of point defects, small defect clusters are also likely to be produced in AlN within the collision cascades due to a high density of energy deposition from the heavy-ion irradiation; these clusters are expected to be stable at 145 K and are unlikely to recover during the irradiation. For lighter-ion irradiation, the recombination rate could be closer to that of defect production because fewer defect clusters, if any, are generated during the irradiation. A recent report [5] has shown that disorder saturation in AlN irradiated with Ar^+ ions was attained at low disorder levels of 0.05–0.15 over a wide range of dose, and the behaviour has been interpreted as due to defect overlapping and recombination during the ion irradiation. The presence of the disorder saturation stage in this study occurs at a much higher level (~0.7). The result suggests that the Al interstitials (and also N interstitials, see below) produced during the Au^+-ion irradiation at 145 K are mobile in the irradiated crystal structure. This is not unexpected because self-interstitial atoms in Si-irradiated AlN were found to be mobile even at 80 K [16]. Similar behaviour of disorder saturation in GaN irradiated with O^+ [17] and Au^+ ions [18] was also observed at medium-high doses and was attributed to the

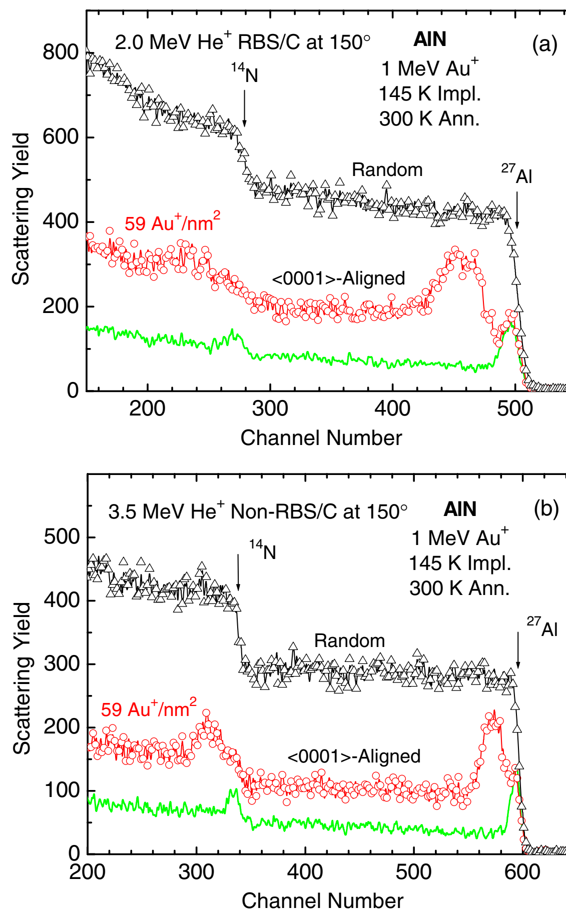

Figure 4. ⟨0001⟩-aligned spectra for AlN irradiated to an ion fluence of 59 Au$^+$ nm^{-2} at 145 K and subsequently annealed at 300 K for 72 h, obtained from (a) 2.0 MeV He$^+$ RBS/C and (b) 3.5 MeV He$^+$ non-RBS/C. Also included are random and ⟨0001⟩-aligned spectra from a virgin area.

mobile interstitials that migrated and accumulated or annihilated at the surface and dislocation loops [19, 20]. Similarly, the disorder saturation in AlN may also be a result of rapid interstitial migration and efficient annihilation, as will be further discussed in section 3.2.

In order to simultaneously study disorder on both the Al and N sublattices in AlN, a resonant He$^+$-ion scattering for N was selected. At an incident energy of 3.2–3.5 MeV for analysis of the disorder region, the cross section for N at a scattering angle of 165° is flat, with a value increased by a factor of ∼1.6 as compared to 2.0 MeV He$^+$ RBS, while that for Al remains nearly unchanged [21]. Figure 4 shows a comparison of the scattering spectra of the 2.0 MeV He$^+$ RBS/C and 3.5 MeV He$^+$ non-RBS/C for the same AlN sample irradiated to an ion fluence of 59 Au$^+$ nm^{-2} at 145 K. Although the Al damage peak is distinctive and can be readily used for disorder analysis from the conventional RBS/C, the N damage peak is not well resolved. In contrast, both the Al and N peaks are well defined in the case of 3.5 MeV He$^+$ non-RBS/C, which provides a convenient means to analyse the disorder on both the Al and N sublattices in AlN.

The relative disorder at the depth of 104 nm on the Al and N sublattices in AlN irradiated at 145 K and stored at room temperature for ∼72 h is shown in figure 5. These data were

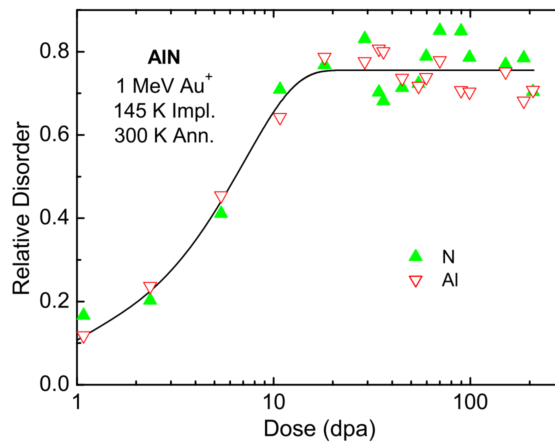

Figure 5. Relative disorder on both the Al and N sublattices, observed along the ⟨0001⟩ axis, as a function of dose at the depth of 104 nm in AlN irradiated at 145 K and subsequently annealed at room temperature for 72 h.

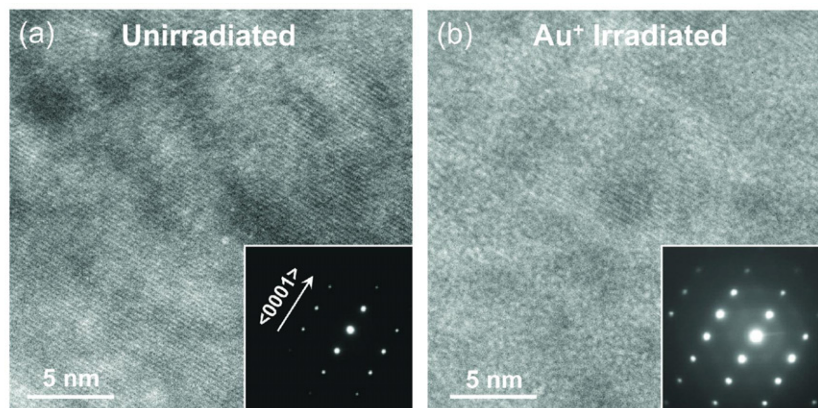

Figure 6. HRTEM micrographs for (a) a bulk area in the unirradiated AlN and (b) a region of disorder saturation in AlN irradiated to 366 Au^+ nm^{-2} at 145 K and stored at room temperature. The inset images show the selected-area electron diffraction patterns for the samples.

obtained using a straight-line approximation for subtracting the dechannelling contributions, which is simpler for extracting the disorder on the N sublattice and leads to similar values of disorder at the damage peak as compared to the iterative procedure that was used for figures 2 and 3. From figure 5, the two data sets follow the same curve (solid line) within experimental error. This result suggests that the disordering behaviour for the two sublattices observed along the ⟨0001⟩ axis in the irradiated AlN is similar over the applied doses ranging from 1 to 208 dpa at 145 K. Some small differences between the data in figures 3 and 5 could originate from depth deviation and data analysis.

3.2. Microstructures of the irradiated AlN

Figure 6 shows the high-resolution cross-sectional TEM images with the zone axis $[1\bar{1}00]$ for unirradiated and irradiated AlN. For the unirradiated sample in the bulk shown in figure 6(a),

clear basal-plane fringes are exhibited without much planar distortion or dislocations observed. Some grey contrast in the image is caused by the local lattice stress. The inserted electron diffraction image shows a pattern of bright spots with the ⟨0001⟩ axis indicated. The diffraction pattern suggests that there is only one crystalline phase involved without amorphous materials. Slightly stretched spots outside the centre confirm the small lattice stress. These results suggest that the sample had a high crystalline quality in the bulk. In contrast, the irradiated AlN in figure 6(b) at the depth of disorder saturation (366 Au^+ nm^{-2} at 145 K) shows both nanoscale crystalline and amorphous domains. These crystalline domains are well aligned with the substrate crystal. Unlike polycrystalline materials with a random distribution of orientation, which is equivalent to an amorphous material from the ion-channelling point of view, such an aligned structure contributes to the channelling effects, as illustrated in figure 1. The diffraction pattern in figure 6(b) shows diffuse bright halos that are characteristic of amorphous materials, in addition to the regular bright spots from the crystalline AlN, which is consistent with the observation of the HRTEM image (figure 6(b)).

Apparently, the amorphous phase was not produced by a single-ion cascade or direct impact process because the dose in this depth region has reached 180 dpa. This is consistent with a recent report [5] that has indicated that a single Ar^+-ion impact in AlN produces only point defects due to a high force constant and a low cross section for damage production. It is likely that the local amorphization in AlN (figure 6(b)) at the high dose was achieved as a result of defect interaction and defect-stimulated processes. It may be worthwhile to note that the microstructure in figure 6(b) is different from what was observed for the ion-irradiated GaN that showed a high density of dislocation loops (stacking faults) [19, 22] in the disorder saturation regime and randomly oriented crystalline domains [19] at higher doses. Since the crystalline domains in figure 6(b) have a dimension of the order of only 10 nm or less, interstitials produced within the crystalline domains could diffuse rapidly to the crystalline/amorphous interfaces that serve as effective sinks for them. In addition, some interstitials may combine with uncorrelated vacancies or be absorbed by dislocation loops on their pathway to the interface. Besides, it cannot be excluded, in principle, that vacancies within the crystalline domains undergo similar processes. These interstitial processes, and possibly vacancy processes as well, are believed to contribute to the nearly perfect balance between the defect formation and annihilation, which is responsible for the disorder saturation in AlN during the Au^+ irradiation. In general, the more mobile the point defects are and the lower the dose rate is, the larger the retained crystalline domains should be.

3.3. Dopant behaviour

The atomic percentage of the implanted Au in AlN is plotted in figure 7 as a function of depth for various ion fluences at 145 K. With the increase of ion fluence, the Au peak gradually shifts towards the surface. At low fluences (5.4 Au^+ nm^{-2} and lower), the Au peak maximum is located at ∼107 nm. A total depth shift of ∼26 nm to a lower value occurs at the ion fluence of 424 Au^+ nm^{-2}. This shift originates primarily from ion sputtering of the surface during the Au^+ irradiation. Experimentally, both optical interferometry and step-height profilometry measurements for the irradiated spots with the high fluences were attempted, but neither of the techniques could accurately determine the crater depth. This is partly due to material transparency and surface roughness. For the spot with the highest ion fluence (424 Au^+ nm^{-2}), the crater depth is expected to be ∼26 nm (figure 7).

Also expected from the sputtering effects is the Au peak broadening. The experimental data indicate that there is a nearly linear dependence of the full width at half maximum (FWHM) on ion fluence over the applied fluence range in this study. The FWHM of the Au

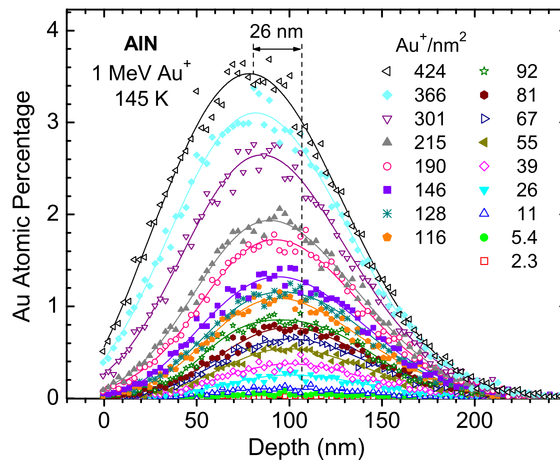

Figure 7. Depth profiles of the implanted Au in AlN obtained from the spectra shown in figure 1 and other unplotted spectra. The solid lines are the Gaussian fits to the data.

profile in figure 7 increases from 90 nm at 2.3 Au^+ nm^{-2} to 115 nm at 424 Au^+ nm^{-2}. This represents a width broadening of 25 nm, which is numerically comparable to the peak shift of 26 nm for the highest fluence. The result suggests that a significant Au diffusion during the ion irradiation did not occur during the ion irradiation. After sample storage at room temperature for 72 h, measurements for the Au profiles were repeated. There is no evidence that shows any measurable diffusion of the Au in the irradiated AlN (data not shown). In addition, the analysing beam of either 2 or 3.5 MeV He^+ ions does not promote Au diffusion at room temperature. This behaviour is similar to that of the Au implants in SiC [23], but exhibits a sharp contrast to that in GaN, where both the Au and N were found to diffuse towards the surface during ion irradiation or thermal annealing [20, 24].

4. Summary

The disordering behaviour on the Al and N sublattices in AlN is similar, exhibiting a gradual increase in the disorder level below a dose of 10 dpa, followed by a disorder saturation at a level of ~0.7 over a wide dose range from 15 to 208 dpa. A continuously amorphized layer is not formed in AlN irradiated up to the highest dose at 145 K. It appears that Al interstitials tend to diffuse towards the bulk during the Au^+-ion irradiation at low temperature. The primary microstructural features at the disorder saturation stage are the coexistence of nanoscale amorphized and aligned crystalline domains. The interstitials produced during the Au^+-ion irradiation in AlN at 145 K are highly mobile and can readily diffuse and annihilate at the crystalline/amorphous interfaces. On their pathway, interstitials could combine with uncorrelated vacancies or be absorbed by dislocation loops to recover the defects. Similar processes for vacancies cannot be excluded in principle. These processes are believed to contribute to the observed disorder saturation. In addition, the disorder produced at 145 K is stable at room temperature, even with the presence of the He^+-ion irradiation. The implanted Au in AlN does not diffuse significantly during ion irradiation at 145 K or during room-temperature annealing. The energetic He^+ beams also do not promote Au diffusion in the irradiated AlN at room temperature.

Acknowledgments

This work was supported by the Division of Materials Sciences and Engineering, Office of Basic Energy Sciences, US Department of Energy, under Contract DE-AC05-76RL01830. Support for the accelerator and TEM facilities within the Environmental Molecular Sciences Laboratory (EMSL) at the Pacific Northwest National Laboratory (PNNL) was provided by the Office of Biological and Environmental Research, US Department of Energy.

References

[1] Ponce F A and Bour D P 1997 *Nature* **386** 351–9
[2] Taniyasu Y, Kasu M and Makimoto T 2006 *Nature* **441** 325–8
[3] Clinard F W Jr 1979 *J. Nucl. Mater.* **85/86** 393–404
[4] Yano T and Iseki T 1993 *J. Nucl. Mater.* **203** 249–54
[5] Wendler E and Wesch W 2006 *Nucl. Instrum. Methods Phys. Res.* B **242** 562–4
[6] Kucheyev S O, Williams J S, Zou J, Jagadish C, Pophristic M, Guo S, Ferguson I T and Manasreh M O 2002 *J. Appl. Phys.* **92** 3554–8
[7] Hu Q, Tanaka S, Yoneoka T and Noda T 2000 *Nucl. Instrum. Methods Phys. Res.* B **166/167** 70–4
[8] Ronning C, Dalmer M, Uhrmacher M, Restle M, Vetter U, Ziegeler L, Hofsäss H, Gehrke T, Järrendahl K, Davis R F and ISOLDE Collaboration 2000 *J. Appl. Phys.* **87** 2149–57
[9] Thevuthasan S, Peden C H F, Engelhard M H, Baer D R, Herman G S, Jiang W, Liang Y and Weber W J 1999 *Nucl. Instrum. Methods Phys. Res.* A **420** 81–9
[10] McCready D E, Thevuthasan S and Jiang W 1999 *Applications of Small Accelerators in Research and Industry* ed J L Duggan and I L Morgan (New York: American Institute of Physics) pp 537–40
[11] Swanson M L 1995 *Handbook of Modern Ion Beam Materials Analysis* ed J R Tesmer and M Nastasi (Pittsburgh, PA: Materials Research Society) p 267
[12] Jiang W, Weber W J, Wang C M, Wang L M and Sun K 2004 *Defect Diffus. Forum* **226–228** 91–112
[13] Zhang Y, Weber W J, Shutthanandan V and Thevuthasan S 2006 *Nucl. Instrum. Methods Phys. Res.* B **251** 127–32
[14] Ziegler J F, Biearsack J P and Littmark U 1985 *The Stopping and Range of Ions in Solids* (New York: Pergamon) available from: http://www.SRIM.org/
[15] Pells G P 1988 *J. Nucl. Mater.* **155–157** 67–76
[16] Zinkle S J, Snead L L, Eatherly W S, Jones J W and Hensley D K 1999 *Mater. Res. Soc. Symp. Proc.* **537** G6.15
[17] Jiang W, Weber W J, Thevuthasan S, Exarhos G J and Bozlee B J 1999 *Mater. Res. Soc. Symp. Proc.* **540** 305–10
[18] Jiang W, Weber W J and Thevuthasan S 2000 *J. Appl. Phys.* **87** 7671–8
[19] Jiang W, Weber W J, Wang L M and Sun K 2004 *Nucl. Instrum. Methods Phys. Res.* B **218** 427–32
[20] Jiang W, Zhang Y, Weber W J, Lian J and Ewing R C 2006 *Appl. Phys. Lett.* **89** 021903
[21] Cox R P, Leavitt J A and McIntyre L C Jr 1995 *Handbook of Modern Ion Beam Materials Analysis* ed J R Tesmer and M Nastasi (Pittsburgh, PA: Materials Research Society) p 499, 504
[22] Wang C M, Jiang W, Weber W J and Thomas L E 2002 *J. Mater. Res.* **17** 2945–52
[23] Jiang W, Wang C M, Weber W J, Engelhard M H and Saraf L V 2004 *J. Appl. Phys.* **95** 4687–9
[24] Kucheyev S O, Williams J S and Pearton S J 2001 *Mater. Sci. Eng.* R **33** 51–108